Journal of Hydrology: Regional Studies 35 (2021) 100808

Contents lists available at ScienceDirect

Journal of Hydrology: Regional Studies

journal homepage: www.elsevier.com/locate/ejrh

Development of spatially varying groundwater-drawdown functions for land subsidence estimation

Hone-Jay Chu [a,*], Muhammad Zeeshan Ali [a], Tatas [a], Thomas J. Burbey [b]

[a] National Cheng Kung University, Taiwan
[b] Virginia Polytechnic Institute and State University, United States

ARTICLE INFO

Keywords:
Subsidence estimation
Spatial regression
Drawdown
Groundwater

ABSTRACT

Study region: Choshui River alluvial fan, Taiwan.
Study focus: Land subsidence caused by groundwater overexploitation is a critical global problem. The spatial distribution of land subsidence is crucial for effective environmental management and land planning in subsidence prone areas. Because of the nonlinear relationship between subsidence and drawdown due to groundwater exploitation in heterogeneous aquifers, a spatial regression (SR) model is developed to effectively estimate nonlinear and spatially varying land subsidence. Considering various data inputs in the Choshui River alluvial fan, the SR model offers a robust method for accurately estimating the spatial patterns of subsidence using only drawdown as input data.
New hydrological insights for the region: Without requiring extensive calibration or an elaborate numerical groundwater flow and subsidence model, the model provides annual subsidence patterns using a spatially varying relationship between drawdown and resulting land subsidence. Results show that the largest water-level cone of depression occurs in the distal fan area. Nonetheless, the calculated subsidence bowl closely approximates the observed one located much farther inland. The root-mean-square-errors (RMSEs) of annual subsidence is less or equal to 0.76 cm for the SR. Results indicate that the SR model reasonably estimates the spatial distribution of the skeletal storage coefficient in the aquifer system. The large coefficient that represents high potential of inelastic compaction occurs in the southern inland area, whereas the small coefficient that represents elastic compaction occurs in the northern area and proximal fan. Furthermore, this method can be used efficiently for subsidence management/ regulation and might be widely used for subsidence estimation solely based on drawdown.

1. Introduction

Land subsidence caused by excessive groundwater exploitation is a severe problem in numerous cities and regions, including Shanghai (Shen and Xu, 2011; Xu et al., 2016), Mexico City (Kirwan and Megonigal, 2013), Bangkok (Phien-Wej et al., 2006), Iran (Amiraslani and Dragovich, 2011; Rahmati et al., 2019), Las Vegas (Bell et al., 2008; Hoffmann et al., 2001) and the San Joaquin Valley in California (Faunt et al., 2016; Jeanne et al., 2019; Poland, 1972; Smith and Majumdar, 2020). These areas with problematic

* Corresponding author at: National Cheng Kung University, No.1, University Road, Tainan City, 701, Taiwan.
E-mail addresses: honejaychu@geomatics.ncku.edu.tw (H.-J. Chu), p68077064@mail.ncku.edu.tw (M.Z. Ali), tatas@ce.its.ac.id (Tatas), tjburbey@vt.edu (T.J. Burbey).

https://doi.org/10.1016/j.ejrh.2021.100808
Received 21 October 2020; Received in revised form 10 February 2021; Accepted 5 March 2021
Available online 22 March 2021

subsidence have long been monitored; their distribution and extent of subsidence and water-level decline are well established as the result of the compaction of fine-grained aquitards and interbeds due to aquifer overexploitation (Bonì et al., 2016). The removal of water from storage in fine-grained silts and clays, interbedded within the aquifer system, causes these highly compressible sediments to compact and cause land subsidence. Furthermore, large-scale groundwater utilization from human activities causes environmental problems (Jeanne et al., 2019; Rahmati et al., 2019), such as land degradation, soil salinization and desertification.

Land subsidence is correlated with variations of the aquifer system pore pressures or water-level response to pumping (Burbey, 2001). The drawdown of water levels leads to land subsidence from over-extraction of groundwater (Bell et al., 2008; Galloway and Burbey, 2011). However, generating the subsidence–drawdown relation is critical to better understand and predict the spatial distribution of land subsidence. Accurate modeling requires observations of land deformation and water levels over months to years of time (Faunt et al., 2016; Kim, 2000; Yan and Burbey, 2008). To model the subsidence–drawdown relation, traditional numerical groundwater flow models such as MODFLOW (Mahmoudpour et al., 2016; Shearer, 1998; Zhou et al., 2003) combined with a post-processing software package such as GMS (Parhizkar et al., 2015) can provide water-level and flow distributions of the system under observation. Thus, land subsidence can be simulated from changes in water pressure within the aquifer system coupled with the SUB Package (Hoffmann et al., 2003b). A coupled numerical model that incorporates the concepts of three dimensional poroelasticity based on Biot's consolidation theory (Biot, 1941, 1955) is developed for simulating three dimensional displacement of solids within unconsolidated aquifers in response to induced changes in water pressure (Burbey, 2006; Burbey and Helm, 1999). Elastic (recoverable) and inelastic (permanent) compaction from stress–strain diagrams (Epstein, 1987; Hanson, 1989; Riley, 1969) can be

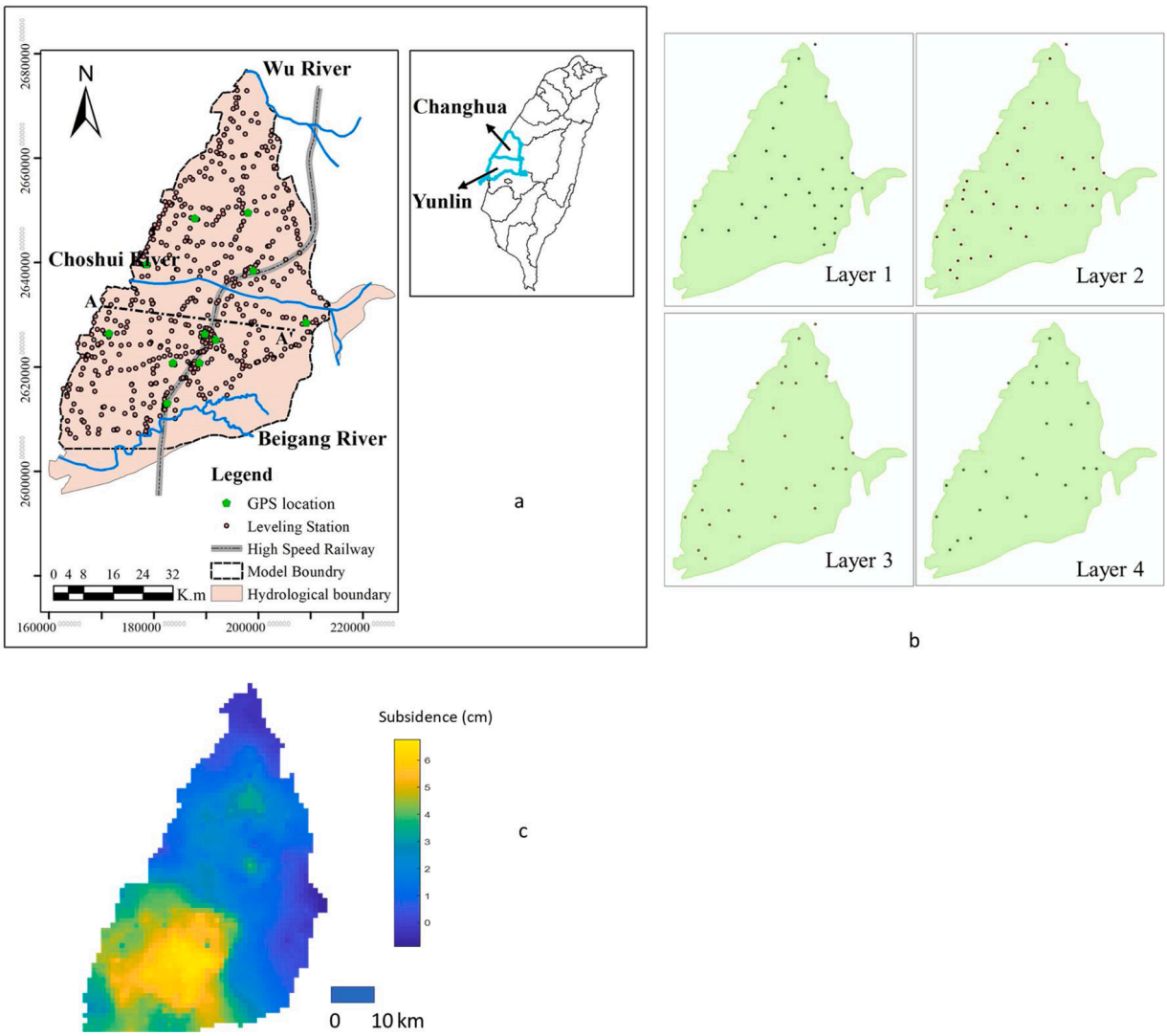

Fig. 1. a). Map showing the location of the study area and observation network, which includes leveling stations (orange circle); (b) Groundwater table observations in four layers (c) Interpolated annual subsidence for 2015 (unit: cm/ year). This IDW interpolation is based on observed leveling data.

identified. Fine-grained sediments tend to compact inelastically if the effective stress exceeds the preconsolidation stress. Decreasing hydraulic heads, such as by increasing effective stresses, causes a small amount of elastic compaction if the effective stress remains less than the preconsolidation stress (Galloway and Burbey, 2011). However, uncertainty still exists in nonspatial models because heterogeneous geological variables cannot be in the same condition that occurs in nature.

Reasonable estimates of the subsidence–drawdown relation can be obtained from regression models using land subsidence and drawdown data, provided sufficient subsidence data and water-level records are available for the area of investigation (Yan and Burbey, 2008). However, drawdown and subsequent compaction of compressible hydrogeologic layers can result in spatially non-uniform and heterogeneous land subsidence of the hydrogeological system (Galloway et al., 1998a; Hoffmann et al., 2003a; Teatini et al., 2006). The subsidence–drawdown relation is rarely well correlated and therefore seldom readily applied in multi-linear regression analyses (Jiang et al., 2015). Moreover, the subsidence–drawdown function is found to be far more heterogenous than most previous studies suggest (Sundell et al., 2019). Spatial regression (SR), i.e. geographically weighted regression (GWR), is a local form of linear regression used to model spatially varying relationships (Fotheringham et al., 2003). Such methods are powerful for capturing the effects of spatially heterogeneous processes and can identify spatial nonstationarity in the subsidence–drawdown relation by allowing regression coefficients to vary spatially. However, previous studies on SR merely consider the relationship between subsidence and groundwater level variation at starting and ending times without considering any compaction processes (Shang et al., 2011).

The present study aims to estimate the spatially variable land subsidence distribution based on annual drawdown between ground-based observations and to improve the limitations of linear regression methods, which typically fail in spatial hydrogeologic settings. The SR-based method is developed in this study to model the spatial relationship between annual drawdown and the resulting land subsidence. The model coefficients are expected to provide the spatial patterns of elastic and inelastic storage coefficients of the aquifer. In addition, a spatial subsidence map is proposed based on only the groundwater drawdown distributions in the aquifer system.

2. Study area and data

2.1. Study area

The Choshui River alluvial fan is located in the mid-western coast of Taiwan and includes the counties of Changhua and Yunlin. The Choshui River runs from east to west through the study area (Fig. 1a), which covers approximately 1800 km^2, and bisects the two counties. The alluvial plain is surrounded by natural geographical boundaries that include the Taiwan Strait to the west, the Central Mountain Ridge to the east, the Wu River to the north, and the Beigang River to the south (Yu and Chu, 2010). The measured groundwater levels of the aquifers indicate that the system has two major flow directions, one from the eastern mountain area to the northwest in Changhua and the other in a southwest direction in Yunlin.

Fig. 2 shows a hydrogeological profile of the Choshui River alluvial fan that comprises Aquifers I, II-1, II-2, III, and IV (F1–F4 in Fig. 2) measured from the land surface downward. Aquitards (T1–T3) separate the aquifers. Aquifers I, II-1, II-2, III are layers 1, 2, 3, 4 in the later. Aquitards are most relevant in the distal-fan and mid-fan areas and gradually diminish in thickness toward the east. The proximal-fan represents the major recharge area of the aquifer system (Jang et al., 2008; Yu and Chu, 2010).The distribution of sediments in the alluvial fan transitions from largely gravel, to sand, and then to clay from the proximal fan to the distal fan. Moreover, Aquifer II is the major aquifer of the Choshui alluvial plain because of its large spatial extent and acceptable depth for groundwater

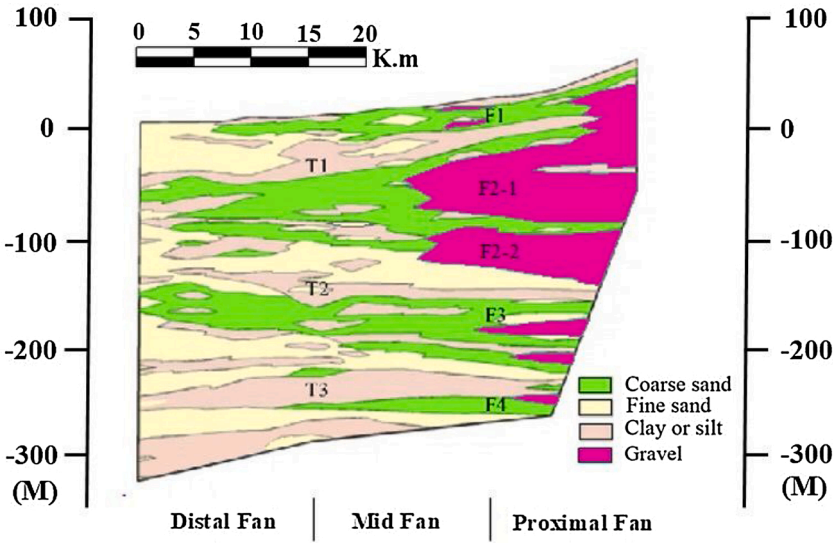

Fig. 2. Hydrogeological profile in the Choshui River alluvial fan in an east–west direction, A–A' (Central Geological Survey, 1999).

extraction (Liu et al., 2004; Yu and Chu, 2010).

Given the insufficient surface water supply in the alluvial fan, residents extract groundwater to supplement their demands for irrigation, aquaculture, and household domestic use, especially in dry seasons. Groundwater is the major source of water for civilian and agricultural use and represents approximately 240,000 m^3/day in the study area. The majority of water is used in agriculture, such as rice paddies, with 1.8 and 1.5 billion cubic meters per year on average for Changhua and Yunlin, respectively (Lee et al., 2018). Groundwater overdraft causes serious land subsidence in the area, especially during droughts. An area of approximately 300 km^2 experiences significant subsidence (> 3 cm/year in 2015), despite the enforced restrictions on groundwater exploitation. Fig. 1c shows spatial pattern of observed annual land subsidence from all aquifer layers.

2.2. Required data for this investigation

This investigation uses monthly groundwater level observations in 2015. The water-level observations of aquifer layers 1, 2, 3, and 4 obtained from 33, 40, 28, and 28 monitoring wells, respectively, are evenly distributed over the entire Choshui River alluvial fan (Fig. 1a).

In addition, annual subsidence rates for 2015 from 662 leveling points (Fig. 1a) have been collected. A leveling network amounting to over 1,000 km in length is used to calculate subsidence for every 1.5 km interval along the leveling routes. Leveling specifications satisfy a loop closure of less than 3 $\sqrt{K}$ mm, where K is the length of the leveling circuit in kilometers. The vertical accuracy of leveling data is generally within 1 cm (Hung et al., 2010). Leveling has a high degree of accuracy but is time consuming and expensive compared with GPS. The leveling and groundwater level data are obtained from the Water Resources Agency of Taiwan. Fig. 1b shows groundwater table observations in four layers. In addition, GPS data and InSAR deformation maps are also used to visually check the calibrated data produced in this study.

3. Data analysis methods

3.1. Model development

Based on Terzaghi's principle of effective-stress (Hoffmann et al., 2003a), the nonlinear stress–compaction relation is typically linearized with respect to preconsolidation stress (Shen and Xu, 2011; Smith and Majumdar, 2020). The calculation of total aquifer system compaction (subsidence) can be linearized where incremental changes in effective stress (hydraulic head) are typically small, as

$$\Delta z = S_k \Delta h, \tag{1}$$

where Δz is the subsidence, S_k is the skeletal storage coefficient, and Δh is the change in hydraulic head. If the effective stress remains less than the preconsolidation stress (or less than the past maximum drawdown), the compaction is entirely elastic. In this study, the soil rebound (volume expansion after removal of mechanical stress) is disregarded from Δh, which represents the annual cumulative drawdown or the total annual change in hydraulic head (Chu and Chang, 2009). Rebound tends to be less than 10 % of the original subsidence (Chaussard et al., 2014a). The total annual drawdown is then stated as:

$$\Delta h = \sum_t \Delta h_t, \tag{2}$$

where $\Delta h_t = h_{t+1} - h_t$ if $h_{t+1} < h_t$. In this one-year case, the time step t varies from 1 to 12 representing the months of the year.

Subsidence is a function of accumulated drawdown (Ali et al., 2020). Furthermore, a regression expression identifies the relation between subsidence and groundwater level. Eq. (1) is extended to yield an estimate of subsidence at observation i in a multi-layer aquifer, which can be expressed as:

$$\Delta z_i = \sum_l S_{kl} \Delta h_{il} + \varepsilon_i, \tag{3}$$

where l is the layer number in the multi-layer aquifer, S_{kl} is the lth skeletal storage coefficient in a multi-layer system and Δz_i is the land subsidence at observation i. This study uses the annual subsidence rate for 2015 and Δh_{il} is the estimated total groundwater decline (drawdown) at observation i from aquifer layer l. ε_i is the residual of the regression model. Eq. (3) is further extended to allow for spatially varying subsidence and drawdown in a multi-layer aquifer system as follows:

$$\Delta z_i = \sum_l S_{kl}(u_i, v_i) \Delta h_{il} + \varepsilon_i, \tag{4}$$

where $S_{kl}(u_i, v_i)$ varies with the spatial coordinates (u_i, v_i) at observation i in the lth layer. This spatial coefficient $S_{kl}(u_i, v_i)$ in Eq. (4) represents the skeletal storage coefficient in each aquifer, which is required to accurately estimate subsidence from drawdown. Eq. (4) exploits the spatial dimension by using the positive autocorrelation between neighboring observations in space and in this way accommodates spatial autocorrelation (Stojanova et al., 2012).

3.2. Spatial coefficient estimation and model validation

The SR is an extension of ordinary least squares (OLS) (Fotheringham et al., 2003). Using the SR, the estimated parameter matrix $\widehat{\beta}(u_i, v_i)$, which includes $S_{kl}(u_i, v_i)$ at each observation i is expressed as:

$$\widehat{\beta}(u_i, v_i) = \left[H^T \mathrm{W}(u_i, v_i) H\right]^{-1} H^T \mathrm{W}(u_i, v_i) Z, \tag{5}$$

where

$$H = \begin{bmatrix} \Delta h_{11} & \Delta h_{12} \cdots & \Delta h_{1L} \\ \vdots & \ddots & \vdots \\ \Delta h_{n1} & \Delta h_{n2} \cdots & \Delta h_{nL} \end{bmatrix}, Z = \begin{bmatrix} \Delta z_1 \\ \vdots \\ \Delta z_n \end{bmatrix}, \tag{6}$$

$$\mathrm{W}(u_i, v_i) = diag\left(w_1(\mathrm{i}),\ \ldots w_j(\mathrm{i}) \ldots, w_n(\mathrm{i})\right), \tag{7}$$

and

$$\widehat{\beta}(u_i, v_i) = (S_{k1}(u_i, v_i), S_{k2}(u_i, v_i), \ldots, S_{kL}(u_i, v_i))^T. \tag{8}$$

H and Z represent the matrix form of Δh_{il} and Δz_i for the n observations and L layers used in this study. $\mathrm{W}(u_i, v_i)$ is a spatial weight matrix based on the Euclidean and Gaussian distance decay-based functions in the spatial domain. In this case, the Euclidean distance is expressed in meters. The parameter $w_j(\mathrm{i})$ between observations i and neighboring j in the spatial weight matrix is commonly used as a kernel and represents a Gaussian distance decay-based function, $w_j(\mathrm{i}) = exp\left(-\frac{D_{ij}^2}{b^2}\right)$, where D_{ij} is the Euclidian distance between observations i and j. $\mathrm{D}_{ij} = \sqrt{(\mathrm{u}_i - \mathrm{u}_j)^2 + (\mathrm{v}_i - \mathrm{v}_j)^2}$ and b is the non-negative parameter known as the bandwidth (Brunsdon et al., 1996). Bandwidth b can be determined by several criteria, such as the cross validation (CV) procedure (Fotheringham et al., 2003; Chu et al., 2018). The CV procedure is used to select the optimal parameters b:

$$\mathrm{CV}\left(b\right) = \sum_i (\Delta z_i - \Delta z_{\neq i}(b))^2. \tag{9}$$

For comparison, the models for linear and spatial regressions i.e., OLS and SR are applied on all four aquifer layers, including mixed

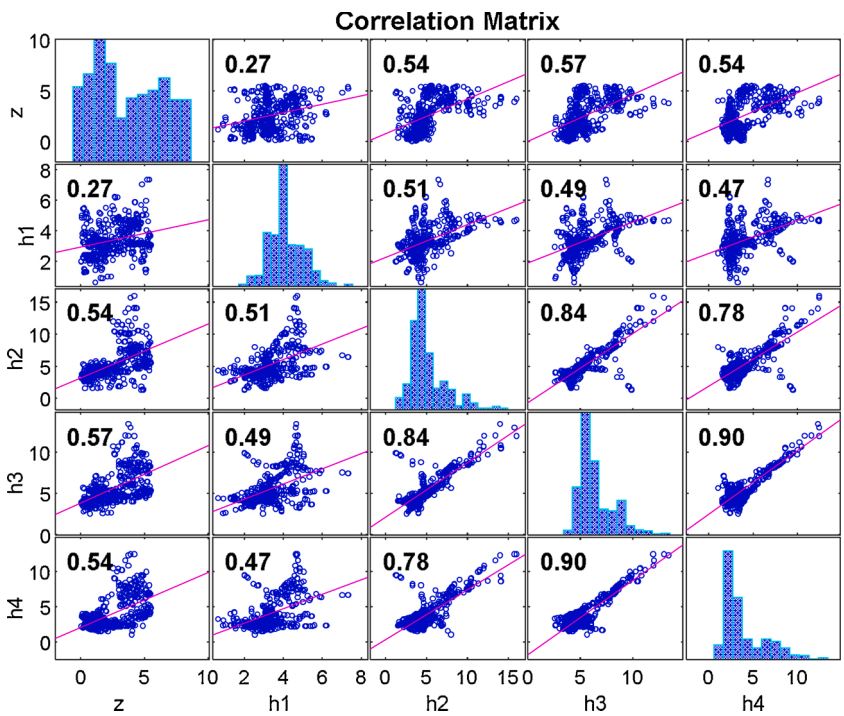

Fig. 3. Correlations between subsidence (z, unit: cm) and groundwater level variations, such as cumulative drawdowns in the four aquifer layers (h1–h4, unit: m).

and single layer drawdowns from different aquifers. Spatial estimation of the drawdown is applied using inverse distance weighting (IDW). The models are developed using MATLAB. Model 1 is based on the cumulative drawdown from all aquifer layers. Models 2–5 are based on only drawdowns from Layers 1–4 without the y-intercept, respectively, as shown at a later stage.

The data are split into a training set (80 %) for model calibration, while an independent test set (20 %) is used for validation. To evaluate the model performance, the common measures R^2 and RMSEs are used on the basis of observation data and estimated values at these points of the test set.

4. Results and discussion

The subsidence–accumulated drawdown relation was built in linear and spatial regressions; that is, the SR model. First, a relation between total subsidence and multi-layer drawdowns was accurately formulated, and the spatial patterns of subsidence were subsequently estimated.

4.1. Overview of subsidence and drawdown

Fig. 3 displays the correlation between subsidence and variations in groundwater level. The subsidence–drawdown relation is

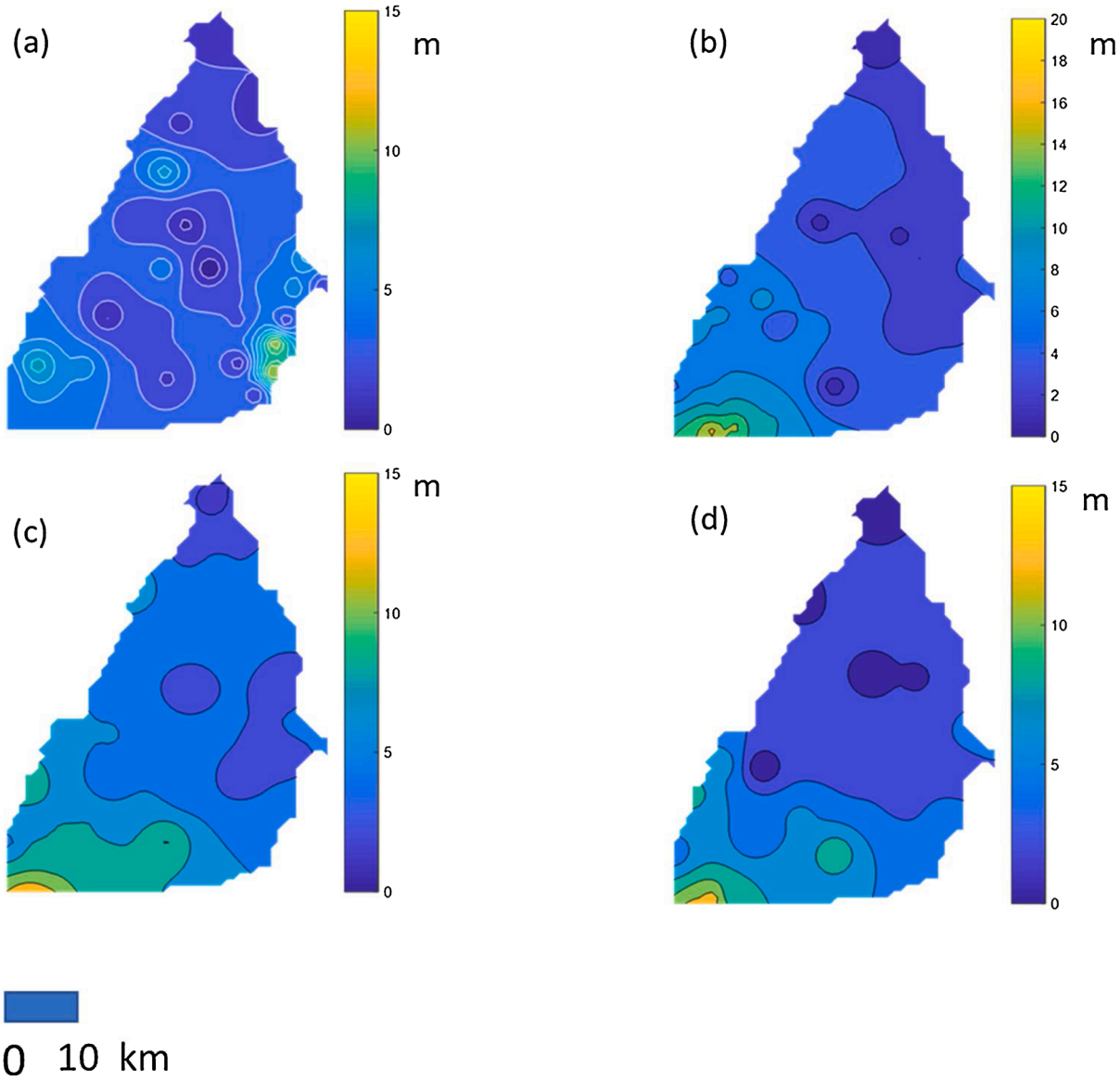

Fig. 4. Annual accumulated groundwater level declines (m) in 2015 in aquifer Layers 1–4 (a–d).

nonlinear (correlation coefficient = 0.27, 0.54, 0.57, and 0.54, respectively, in each of the four aquifer layers). Groundwater drawdowns in Layers 2–4 are similar (correlation coefficient = 0.84 in Layers 2 and 3; 0.78 in Layers 2 and 4). Drawdowns in Layer 1 (unconfined aquifer) vary spatially over shorter distances compared to those of the confined aquifer (Layers 2–4). Figs. 1c and 4 show the spatial distribution of annual observed subsidence and accumulated drawdown, respectively, for 2015, when the maximum annual permanent subsidence is approximately 7 cm (Fig. 1c). The spatial distribution of subsidence reveals a bowl in the central area of Yunlin (Hwang et al., 2008). Within the study area, the maximum accumulated drawdown in Layers 1–4 ranges from 15 to 20 m (Fig. 4). The cumulative drawdowns implies that similar cones of depression are located in Layers 2–4 in the southwest distal fan area, near the coast. Drawdown cones are located along the distal fan and mountain areas in Layer 1. Compared with the four-layer drawdown pattern, the drawdown is greatest in Layer 2 in the study area. In addition, drawdowns in Layers 2–4 are highly correlated (Fig. 3), while Layer 3 is most closely correlated to the subsidence of the four-layer drawdown model (Fig. 3).

The compression behavior of clay agrees with Terzaghi's consolidation theory (Liu et al., 2004). Land subsidence with inelastic compression continues as water levels continuously decline. The inelastic compression of fine-grained aquifer interbeds is likely responsible for the vast majority of subsidence problems, based on the compressibility and total thickness of fine-grained deposits throughout the region (Galloway et al., 1998b; Galloway and Sneed, 2013). The cone of maximum drawdown occurs in the distal fan area, whereas the current major subsidence bowl occurs inland. Consequently, the cone of maximum drawdown fails to fully coincide with the location of the subsidence bowl (Erban et al., 2014). In the coastal area or distal fan area, the rate of pumping is proposed to decrease to stabilize or reduce water level declines. This subsequently reduces land subsidence, given that the largest occurrence in the southern inland area induced by heavy withdrawal of groundwater. This is a sensitive environmental concern because the Taiwan High Speed Rail is constructed through the central subsidence area, which might pose a serious threat to its operation (Hwang et al., 2008; Tung and Hu, 2012).

4.2. Model performance

The performance of SR such as the RMSEs in the multi- or single-aquifer system (RMSE = 0.62–0.76 cm) is better than that of OLS (RMSE = 1.53–2.12 cm) (Table 1). The best models are appear to be Model 1 in the multi-aquifer system and Model 4 in the single-aquifer system. However, the subsidence–drawdown model using OLS is not appropriate due to its poor performance (Table 1). The SR is more accurate than that of OLS. Results of OLS reveal a subsidence–drawdown function with negative a slope for Layer 1 (high drawdown -low subsidence exists in the proximal fan) but a positive slope for Layers 2, 3, and 4 in Model 1 (Table 2). In addition, the RMSEs of Model 4 using OLS and SR are 1.53 and 0.63 cm, respectively. Compared with Models 2–5, the best SR with the lowest RMSEs occurs in Model 4 because the subsidence–drawdown correlation is the highest. However, the poorest OLS model with highest RMSE is Model 2 due to its low subsidence–drawdown correlation (Fig. 3). Validation of our subsidence model with available test data provides consistent and accurate results.

Fig. 5 shows the total estimated land subsidence calculated from linear regression and SR using all-layers (Model 1) and single layer drawdowns (Models 2–5). In a linear regression, the estimated land subsidence bowl occurs in the distal fan area (near the coast), but also in the proximal and distal fan areas in Model 2 due to the variable drawdown patterns occurring in Layer 1. The estimated maximum subsidence in the OLS models occurs at the boundary area of Yunlin, whereas in the SR models subsidence occurs in the inland area of Yunlin (Fig. 5). However, the estimated pattern using OLS does not match the observed subsidence. The SR explicitly considers spatially dependent models to overcome the spatial variability of land subsidence mapping because the SR extends the linear regression by estimating a set of spatial parameters rather than one single set of parameters (Brunsdon et al., 1996; Fotheringham et al., 2003). The model RMSEs are less than or equal to 0.76 cm so that spatial regression can be used to model the spatially varying relation between subsidence and drawdown in the aquifer system.

Model 1 performs the best, but the regression coefficient does not explain the skeletal storage coefficient of each layer independently because land subsidence is a cumulative measurement encompassing all aquifer and aquitard layers. The regression estimate is incapable of distinguishing different hydrogeologic layers. Consequently, we estimate the specific storage on the basis of the drawdown occurring in a single-aquifer system.

4.3. Spatial model coefficient and implication

Fig. 6 exhibits the spatial pattern of regression slope coefficients of the SR in Layers 1–4 for Models 2–5. The regression coefficient distribution varies spatially. The patterns of spatial coefficients are typically similar in Layers 2, 3, and 4. Most coefficients have a positive slope for total drawdown and subsidence (Fig. 6). Only the proximal fan and the area close to Wu River exhibits a negative

Table 1
Model performance comparison for OLS and SR (Model 1: Layers 1–4; Models 2: Layer 1; Models 3: Layer 2; Models 4: Layer 3; (e) Models 5: Layer 4).

	R^2 in OLS	R^2 in SR	RMSE (cm) in OLS	RMSE (cm) in SR
Model 1	0.43	0.98	1.57	0.62
Model 2	−0.01	0.97	2.12	0.76
Model 3	0.33	0.97	1.70	0.73
Model 4	0.36	0.98	1.53	0.63
Model 5	0.31	0.97	1.67	0.74

Table 2
Model coefficients, namely, slopes for OLS and SR (Model 1: Layers 1–4; Models 2: Layer 1; Models 3: Layer 2; Models 4: Layer 3; (e) Models 5: Layer 4).

	Slope in OLS	Average Slope in SR
Model 1	−0.295* (Layer1)	−0.200 (Layer1)
	0.127* (Layer2)	0.156 (Layer2)
	0.472* (Layer3)	0.380 (Layer3)
	0.112* (Layer4)	0.060 (Layer4)
Model 2	0.807* (Layer1)	0.889 (Layer1)
Model 3	0.531* (Layer2)	0.520 (Layer2)
Model 4	0.527* (Layer3)	0.478 (Layer3)
Model 5	0.653* (Layer4)	0.678 (Layer4)

Note: *Coefficient in OLS is statistically significant with p-value < 0.05.

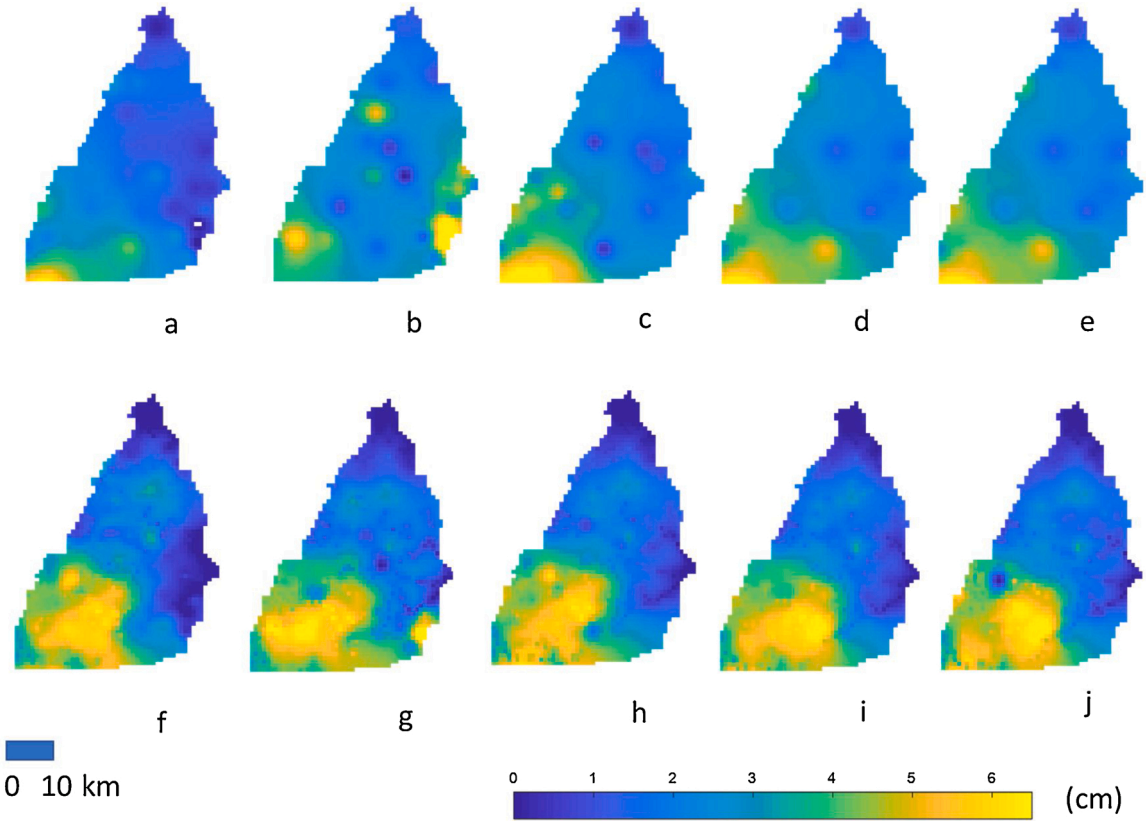

Fig. 5. Estimated annual land subsidence (cm) (a) Layers 1–4; (b) Layer 1; (c) Layer 2; (d) Layer 3; (e) Layer 4 for OLS; and (f) Layers 1–4; (g) Layer 1; (h) Layer 2; (i) Layer 3; and (j) Layer 4 for SR.

relation between the total drawdown and land subsidence (Fig. 6). A negative relation can occur where unloading causes a small soil rebound or where drawdown continues but the subsidence rate declines due to recharge effects (i.e., rainfall, ponds/lakes, canals, and irrigation).

The long-term trend of hydraulic head and vertical displacements are useful to estimate the inelastic skeletal storage coefficient for subsidence features (Miller and Shirzaei, 2015). The spatial patterns of skeletal storage coefficients in four layers can be estimated using the slope coefficients of spatial regression (Fig. 6), which also reflect the skeletal storage coefficients of the aquifers. In Fig. 6(c), the large coefficient value (purple color) represents inelastic compaction in the southern inland area, whereas the small coefficient value (blue color) represents elastic compaction in other areas. The resulting subsidence pattern clearly suggests elasto-plastic mechanical behavior, which includes elastic and inelastic skeletal storage in over-consolidated and normally consolidated soils (Hung et al., 2012; Liu et al., 2004). In recent decades, the excessive pumping of groundwater has resulted in serious subsidence problems along the coast. This subsidence coincides with the increase of aquaculture fisheries since the 1970s. Currently, the rate of compaction in the coastal area is declining. However, the subsidence bowl is moving inland due to over-pumping in this region (Hwang et al., 2008; Chu et al., 2021). Interferometric Synthetic Aperture Radar (InSAR) offers a powerful and useful method for identifying regional land

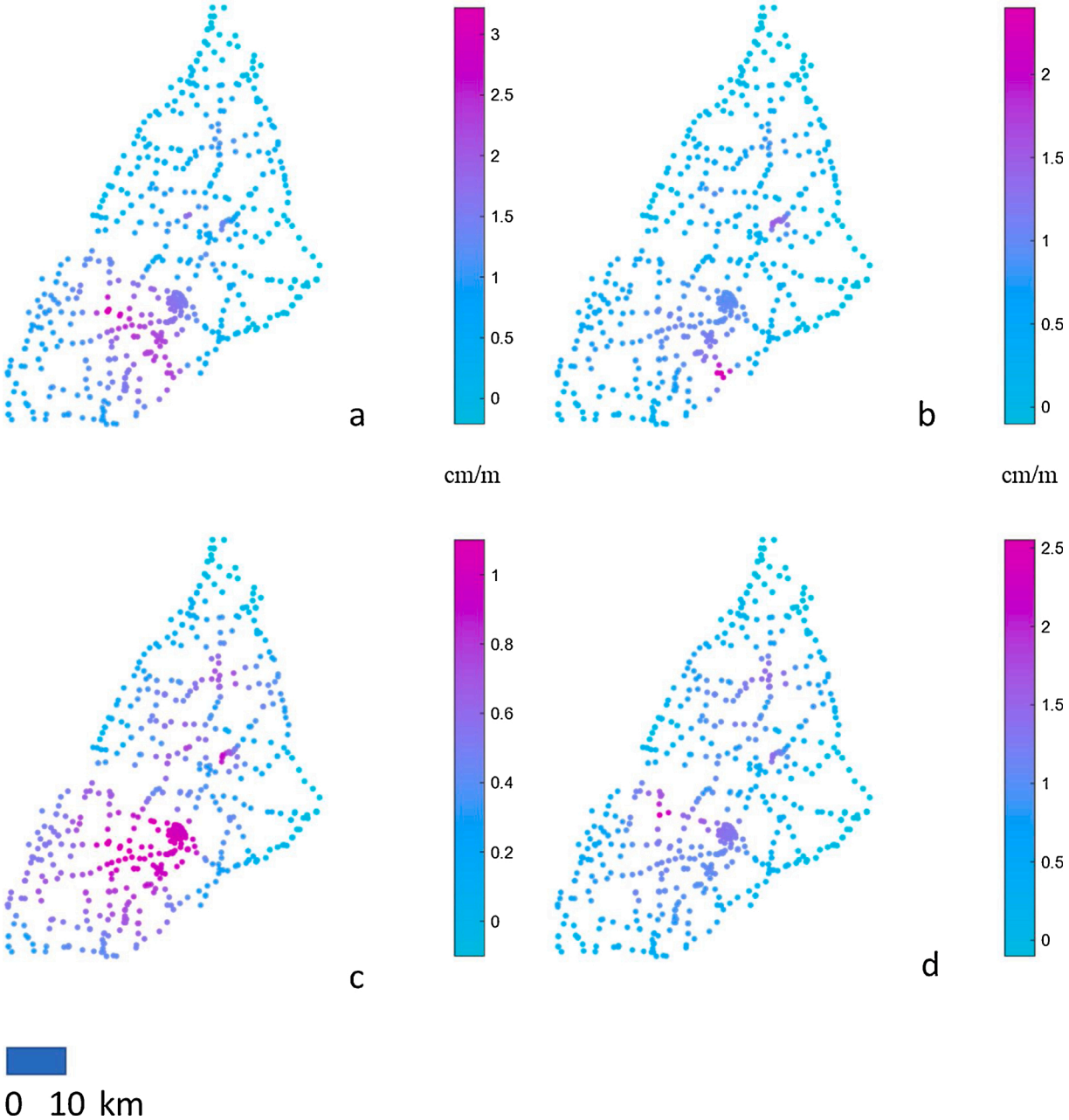

Fig. 6. Spatial coefficients of SR: $S_{kl}(u_i, v_i)$ for (a) Layer 1 in Model 2; (b) Layer 2 in Model 3; (c) Layer 3 in Model 4; and (d) Layer 4 in Model 5 (unit: cm/m).

subsidence (Bürgmann et al., 2000; Bonì et al., 2016; Chaussard et al., 2014b; Galloway et al., 1998b; Hoffmann et al., 2001). The present findings match the results from previous InSAR interferograms for the study region (Tung and Hu, 2012). Moreover, the advent and use of GPS has made land subsidence monitoring more efficient and cost effective. However, GPS is limited because it measures only the surface deformation at point locations (Hosseini et al., 2007). The approach developed in the present study provides robust and reliable maps of estimated land subsidence that are far more spatially descriptive than point-based survey data typically provide.

In the developed models, spatial patterns of subsidence are estimated solely on the basis of drawdown information. The effect of groundwater-level changes on land subsidence can be modeled using a stress–strain relationship with the elastic or inelastic skeletal storage coefficient of the underlying aquifers. However, the entire system includes leveling surveys, borehole extensometer data, and multilayer monitoring of groundwater levels, with the aim to better understand the hydrological and mechanical processes of the aquifer system and to characterize the spatial distribution of land subsidence with a traditional numerical model (Zhang et al., 2014). Characterizing the hydrogeological setting of the aquifer system is a critical step to accomplish this goal (Liu et al., 2004). The

observational data used to characterize hydrogeology is limited (Hubbard and Rubin, 2000) including the hydraulic diffusivity of the confining layer, the distance from the pumping wells, length of the recovery cycle, and the thickness of confining layers. All of these factors can influence the shape of stress–strain hysteresis loops (Burbey, 2001).

In this study, further calibration of the model is not required, unlike other numerical models that typically require an inverse modeling component for calibration purposes. The fundamental benefit of inverse modeling is its ability to automatically estimate parameter values that produce the best fit between observed and simulated hydraulic heads and flows (Franssen et al., 2009; Poeter and Hill, 1997). However, limitations include model uncertainty (hydrogeologic characterization of the system), and measurement and parameter uncertainties (Højberg and Refsgaard, 2005). For example, the numerical model contains parameter uncertainty due to the unknown pumping rates, which can limit the ability to adequately characterize key hydrologic parameters. Therefore, this method can be used efficiently for subsidence management and might be widely used for subsidence estimation solely based on drawdown. Subsidence is influenced by drawdown due to persistent pumping and seasonal variations of groundwater levels from monthly data (Kouda et al., 2015). However, the quality of the drawdown information affects the estimation accuracy of subsidence. This subsidence–drawdown model can be relevant in terms of policy or land subsidence regulation.

5. Conclusions

This study implements a spatial regression-based subsidence-mapping scheme on the basis of groundwater-level observations and offers an effective method to explore the spatial patterns of subsidence through its correlation with drawdowns, without the use of complex hydrogeologic models. The model developed here is based on a SR method and is easy to fit between the total drawdown and subsidence observations. A goodness-of-fit better than OLS (RMSEs are less than or equal to 0.76 cm) is achieved. Without requiring a more detailed hydrogeologic investigation and extensive calibration, this model offers reasonable detail regarding the spatial patterns of land subsidence using a non-linear and spatially varying relationship between the water-level observations and resulting land subsidence. This model can be relevant for water resource policy or land subsidence regulation.

The developed model accurately estimates the spatial pattern of annual land subsidence. The estimated subsidence bowl occurs in the inland area of Yunlin, similar to the actual observed subsidence bowl location. However, the drawdown cone occurs in the coastal area west of the subsidence bowl. The model can estimate the spatial pattern of subsidence that is highly related to the hydrogeological properties and drawdown history, which impacts the location of the observed subsidence bowl. Results also show that the model coefficients accurately reflect the skeletal storage coefficients of the aquifer. The large coefficient value represents inelastic compaction in the southern inland area, whereas the small coefficient value represents the elastic compaction that occurs in the northern area and proximal fan. The coefficient patterns represent elastic and inelastic skeletal storage coefficients in over-consolidated and normally consolidated soils.

In a future study, the recharge effects and hydrodynamic lag that exists between the drawdown and subsequent subsidence can be considered. The effectiveness of the method using fewer observations will be further investigated to determine if the model can be adaptable to areas with a much lower number of observations than used in this study. The prediction of long-term subsidence or subsidence time series can then be investigated.

Author's statement

Hone-Jay Chu: Conceptualization, Methodology, Writing- Original draft preparation. Muhammad Zeeshan Ali and Tatas: Visualization, Investigation, Validation. Thomas J. Burbey: Writing- Reviewing and Editing.

Data availability statement

The data that support the findings of this study are available from Central Geological Survey and Water Resources Agency of Taiwan. Restrictions apply to the availability of the data, which data are available with the official permission.

Declaration of Competing Interest

The authors report no declarations of interest.

Acknowledgements

The authors thank the MOST in Taiwan for their financial support (105-2621-M-006-011-).

The authors also thank Authorea which currently supports the transfer of preprints directly to journals, making the process to submit the work for peer review simpler. Furthermore, the authors would like to thank the editors and anonymous reviewers for providing suggestions of paper improvement.

Appendix A. Supplementary data

Supplementary material related to this article can be found, in the online version, at doi:https://doi.org/10.1016/j.ejrh.2021.100808.

References

Ali, M.Z., Chu, H.J., Burbey, T.J., 2020. Mapping and predicting subsidence from spatio-temporal regression models of groundwater-drawdown and subsidence observations. Hydrogeol. J. 28 (8), 2865–2876.

Amiraslani, F., Dragovich, D., 2011. Combating desertification in Iran over the last 50 years: an overview of changing approaches. J. Environ. Manage. 92, 1–13.

Bell, J.W., Amelung, F., Ferretti, A., Bianchi, M., Novali, F., 2008. Permanent scatterer InSAR reveals seasonal and long-term aquifer-system response to groundwater pumping and artificial recharge. Water Resour. Res. 44.

Biot, M.A., 1941. General theory of three-dimensional consolidation. J. Appl. Phys. 12, 155–164.

Biot, M.A., 1955. Theory of elasticity and consolidation for a porous anisotropic solid. J. Appl. Phys. 26, 182–185.

Bonì, R., Cigna, F., Bricker, S., Meisina, C., McCormack, H., 2016. Characterisation of hydraulic head changes and aquifer properties in the London Basin using Persistent Scatterer Interferometry ground motion data. J. Hydrol. 540, 835–849.

Brunsdon, C., Fotheringham, A.S., Charlton, M.E., 1996. Geographically weighted regression: a method for exploring spatial nonstationarity. Geogr. Anal. 28, 281–298.

Burbey, T.J., 2001. Stress-strain analyses for aquifer-system characterization. Groundwater 39, 128–136.

Burbey, T.J., 2006. Three-dimensional deformation and strain induced by municipal pumping, Part 2: numerical analysis. J. Hydrol. 330, 422–434.

Burbey, T.J., Helm, D.C., 1999. Modeling three-dimensional deformation in response to pumping of unconsolidated aquifers. Environ Eng Geosci. 199–212.

Bürgmann, R., Rosen, P.A., Fielding, E.J., 2000. Synthetic aperture radar interferometry to measure Earth's surface topography and its deformation. Ann. Rev. Earth Planet. Sci. 28, 169–209.

Central Geological Survey, 1999. Project of Groundwater Monitoring Network in Taiwan during First Stage – Research Report of Choushui River Alluvial Fan. Water Resources Bureau press, Taipei County, 383 pp.

Chaussard, E., Bürgmann, R., Shirzaei, M., Fielding, E., Baker, B., 2014a. Predictability of hydraulic head changes and characterization of aquifer-system and fault properties from InSAR-derived ground deformation. J. Geophys. Res. Solid Earth 119, 6572–6590.

Chaussard, E., Wdowinski, S., Cabral-Cano, E., Amelung, F., 2014b. Land subsidence in central Mexico detected by ALOS InSAR time-series. Remote Sens. Environ. 140, 94–106.

Chu, H.-J., Chang, L.-C., 2009. Optimizing capacity-expansion planning of groundwater supply system between cost and subsidence. J. Hydrol. Eng. 15, 632–641.

Chu, H.-J., Kong, S.-J., Chang, C.-H., 2018. Spatio-temporal water quality mapping from satellite images using geographically and temporally weighted regression. Int. J. Appl. Earth Obs. 65, 1–11.

Chu, H.J., Ali, M.Z., Burbey, T.J., 2021. Spatio-temporal data fusion for fine-resolution subsidence estimation. Environ. Model. Softw., 104975

Epstein, V.J., 1987. Hydrologic and geologic factors affecting land subsidence near Eloy, Arizona. Water -Resources Investigations Rep. 87-4143, 28.

Erban, L.E., Gorelick, S.M., Zebker, H.A., 2014. Groundwater extraction, land subsidence, and sea-level rise in the Mekong Delta, Vietnam. Environ. Res. Lett. 9, 084010.

Faunt, C.C., Sneed, M., Traum, J., Brandt, J.T., 2016. Water availability and land subsidence in the Central Valley, California, USA. Hydrogeol. J. 24, 675–684.

Fotheringham, A.S., Brunsdon, C., Charlton, M., 2003. Geographically Weighted Regression: the Analysis of Spatially Varying Relationships. John Wiley & Sons.

Franssen, H.H., Alcolea, A., Riva, M., Bakr, M., Van der Wiel, N., Stauffer, F., Guadagnini, A., 2009. A comparison of seven methods for the inverse modelling of groundwater flow. Application to the characterisation of well catchments. Adv. Water Resour. 32, 851–872.

Galloway, D.L., Burbey, T.J., 2011. Review: regional land subsidence accompanying groundwater extraction. Hydrogeol. J. 19, 1459–1486.

Galloway, D.L., Sneed, M., 2013. Analysis and simulation of regional subsidence accompanying groundwater abstraction and compaction of susceptible aquifer systems in the USA. Boletín de la Sociedad Geológica Mexicana 65, 123–136.

Galloway, D.L., Hednut, K.W., Ingebritsen, S.E., Phillips, S.P., Peltzer, G., Rogez, F., Rosen, P.A., 1998a. InSAR detection of system compaction and land subsidence, Antelope Valley, Mohave Desert, California. Water Resour. Res. 34, 2573–2585.

Galloway, D.L., Hudnut, K.W., Ingebritsen, S., Phillips, S.P., Peltzer, G., Rogez, F., Rosen, P., 1998b. Detection of aquifer system compaction and land subsidence using interferometric synthetic aperture radar, Antelope Valley, Mojave Desert, California. Water Resour. Res. 34, 2573–2585.

Hanson, R.T., 1989. Aquifer-system compaction, Tucson Basin and Avra Valley. U.S. Geological Survey, Arizona.

Højberg, A., Refsgaard, J., 2005. Model uncertainty–parameter uncertainty versus conceptual models. Water Sci. Technol. 52, 177–186.

Hoffmann, J., Zebker, H.A., Galloway, D.L., Amelung, F., 2001. Seasonal subsidence and rebound in Las Vegas Valley, Nevada, observed by synthetic aperture radar interferometry. Water Resour. Res. 37, 1551–1566.

Hoffmann, J., Galloway, D.L., Zebker, H.A., 2003a. Inverse modeling of interbed storage parameters using land subsidence observations, Antelope Valley, California. Water Resour. Res. 39. SBH 5-1 to 5-13.

Hoffmann, J., Leake, S.A., Galloway, D.L., Wilson, A.M., 2003b. MODFLOW-2000 ground-water model–User guide to the subsidence and aquifer-system compaction (SUB) package. Geological Survey Washington DC.

Hosseini, M., Zoej, M.V., Mobasheri, M., Dehghani, M., 2007. Land Subsidence Monitoring Using InSAR and GPS. Map Asia.

Hubbard, S.S., Rubin, Y., 2000. Hydrogeological parameter estimation using geophysical data: a review of selected techniques. J. Contam. Hydrol. 45, 3–34.

Hung, W.-C., Hwang, C., Chang, C.-P., Yen, J.-Y., Liu, C.-H., Yang, W.-H., 2010. Monitoring severe aquifer-system compaction and land subsidence in Taiwan using multiple sensors: yunlin, the southern Choushui River Alluvial Fan. Environ. Earth Sci. 59, 1535–1548.

Hung, W.-C., Hwang, C., Liou, J.-C., Lin, Y.-S., Yang, H.-L., 2012. Modeling aquifer-system compaction and predicting land subsidence in central Taiwan. Eng. Geol. 147, 78–90.

Hwang, C., Hung, W.-C., Liu, C.-H., 2008. Results of geodetic and geotechnical monitoring of subsidence for Taiwan High Speed Rail operation. Nat. Hazards 47, 1–16.

Jang, C.S., Chen, S.K., Ching-Chieh, L., 2008. Using multiple-variable indicator kriging to assess groundwater quality for irrigation in the aquifers of the Choushui River alluvial fan. Hydrol. Process. 22, 4477–4489.

Jeanne, P., Farr, T.G., Rutqvist, J., Vasco, D.W., 2019. Role of agricultural activity on land subsidence in the San Joaquin Valley, California. J. Hydrol. 569, 462–469.

Jiang, Y., Liu, J.-R., Luo, Y., Yang, Y., Tian, F., Lei, K.-C., 2015. Research on critical groundwater level under the threshold value of land subsidence in the typical region of Beijing. Proc. Int. Assoc. Hydrol. Sci. 372, 507–510.

Kim, J.-M., 2000. Generalized poroelastic analytical solutions for pore water pressure change and land subsidence due to surface loading. Geosci. J. 4, 95.

Kirwan, M.L., Megonigal, J.P., 2013. Tidal wetland stability in the face of human impacts and sea-level rise. Nature 504, 53.

Kouda, A., Nagata, K., Sato, T., 2015. Factor analysis on land subsidence in the Nobi Plain, southwest Japan. Proc. Int. Assoc. Hydrol. Sci. 372, 95–99.

Lee, M., Yu, C.-Y., Chiang, P.-C., Hou, C.-H., 2018. Water–energy Nexus for multi-criteria decision making in water resource management: a case study of Choshui River Basin in Taiwan. Water 10, 1740.

Liu, C.-H., Pan, Y.-W., Liao, J.-J., Huang, C.-T., Ouyang, S., 2004. Characterization of land subsidence in the Choshui River alluvial fan, Taiwan. Environ. Geol. 45, 1154–1166.

Mahmoudpour, M., Khamehchiyan, M., Nikudel, M.R., Ghassemi, M.R., 2016. Numerical simulation and prediction of regional land subsidence caused by groundwater exploitation in the southwest plain of Tehran, Iran. Eng. Geol. 201, 6–28.

Miller, M.M., Shirzaei, M., 2015. Spatiotemporal characterization of land subsidence and uplift in Phoenix using InSAR time series and wavelet transforms. J. Geophys. Res. Solid Earth 120, 5822–5842.

Parhizkar, S., Ajdari, K., Kazemi, G.A., Emamgholizadeh, S., 2015. Predicting water level drawdown and assessment of land subsidence in Damghan aquifer by combining GMS and GEP models. Geopersia 5, 63–80.

Phien-Wej, N., Giao, P., Nutalaya, P., 2006. Land subsidence in Bangkok, Thailand. Eng. Geol. 82, 187–201.

Poeter, E.P., Hill, M.C., 1997. Inverse models: a necessary next step in ground-water modeling. Groundwater 35, 250–260.

Poland, J.F., 1972. Land subsidence in the western states due to ground-water overdraft. Water Resour. Bull. 8, 118–131.

Rahmati, O., Golkarian, A., Biggs, T., Keesstra, S., Mohammadi, F., Daliakopoulos, I.N., 2019. Land subsidence hazard modeling: machine learning to identify predictors and the role of human activities. J. Environ. Manage. 236, 466–480.
Riley, F.S., 1969. Analysis of Borehole Extensometer Data from Central California, Vol. 89. International Association of Hydrologic Sciences Publication, pp. 423–431.
Shang, R.-K., Shiu, Y.-S., Ma, K.-C., 2011. Using geographically weighted regression to explore the spatially varying relationship between land subsidence and groundwater level variations: a case study in the Choshuichi alluvial fan, Taiwan. In: Proceedings 2011 IEEE International Conference on Spatial Data Mining and Geographical Knowledge Services. IEEE, pp. 21–25.
Shearer, T., 1998. A numerical model to calculate land subsidence, applied at Hangu in China. Eng. Geol. 49, 85–93.
Shen, S.-L., Xu, Y.-S., 2011. Numerical evaluation of land subsidence induced by groundwater pumping in Shanghai. Can. Geotech. J. 48, 1378–1392.
Smith, R.G., Majumdar, S., 2020. Groundwater storage loss associated with land subsidence in Western United States mapped using machine learning. Water Resour. Res. 56 e2019WR026621.
Stojanova, D., Debeljak, M., Ceci, M., Appice, A., Malerba, D., Džeroski, S., 2012. Dealing with spatial autocorrelation in gene flow modeling. In: Developments in Environmental Modelling, Vol. 25. Elsevier, pp. 35–49.
Sundell, J., Haaf, E., Norberg, T., Alén, C., Karlsson, M., Rosén, L., 2019. Risk mapping of groundwater-drawdown-induced land subsidence in heterogeneous soils on large areas. Risk Anal. 39, 105–124.
Teatini, P., Ferronato, M., Gambolati, G., Gonella, M., 2006. Groundwater pumping and land subsidence in the Emilia-Romagna coastland, Italy: modeling the past occurrence and the future trend. Water Resour. Res. 42.
Tung, H., Hu, J.-C., 2012. Assessments of serious anthropogenic land subsidence in Yunlin County of central Taiwan from 1996 to 1999 by Persistent Scatterers InSAR. Tectonophysics 578, 126–135.
Xu, Y.-S., Shen, S.-L., Ren, D.-J., Wu, H.-N., 2016. Analysis of factors in land subsidence in Shanghai: a view based on a strategic environmental assessment. Sustainability 8, 573.
Yan, T., Burbey, T.J., 2008. The value of subsidence data in ground-water model calibration. Ground Water 46, 438–450.
Yu, H.-L., Chu, H.-J., 2010. Understanding space–time patterns of groundwater system by empirical orthogonal functions: a case study in the Choshui River alluvial fan, Taiwan. J. Hydrol. 381, 239–247.
Zhang, Y., Gong, H., Gu, Z., Wang, R., Li, X., Zhao, W., 2014. Characterization of land subsidence induced by groundwater withdrawals in the plain of Beijing city, China. Hydrogeol. J. 22, 397–409.
Zhou, G., Esaki, T., Mori, J., 2003. GIS-based spatial and temporal prediction system development for regional land subsidence hazard mitigation. Environ. Geol. 44, 665–678.